DEVELOPMENT OF A 15 T NB₃SN ACCELERATOR DIPOLE DEMONSTRATOR AT FERMILAB

I. Novitski, N. Andreev, E. Barzi, J. Carmichael, V. V. Kashikhin, D. Turrioni, M. Yu, and A. V. Zlobin

Abstract— **A 100 TeV scale Hadron Collider (HC) with a nominal operation field of at least 15 T is being considered for the post-LHC era, which requires using the Nb₃Sn technology. Practical demonstration of this field level in an accelerator-quality magnet and substantial reduction of the magnet costs are important requirements for realization of such a machine. Fermilab has started the development of a 15 T Nb₃Sn dipole demonstrator for a 100 TeV scale HC. The magnet design is based on optimized 60-mm aperture 4-layer shell-type coils, graded between the inner and outer layers to maximize the performance and reduce the cost. The experience gained during the Nb₃Sn magnet R&D is applied to various aspects of the magnet design. This paper describes the magnetic and structural designs and parameters of the 15 T Nb₃Sn dipole demonstrator and the steps towards its fabrication.**

Index Terms— **Dipole magnet, collider, magnetic field, mechanical structure, Nb₃Sn superconductor, Rutherford cable.**

I. INTRODUCTION

HADRON COLLIDERS (HC) are the most powerful discovery tools in modern high energy physics. Interest in an HC with energy above the LHC reach has gained further momentum in the strategic plans recently developed in the U.S., Europe and China [1]-[3]. To build a ~100 TeV center of mass energy HC in a ~100 km tunnel, dipoles with a nominal field of ~15 T and ~20% margin operating at 1.9 K or 4.5 K are needed. A nominal field of ~15 T can be provided only by the Nb₃Sn technology. A practical demonstration of this field level in accelerator-quality magnets and a substantial reduction of magnet costs are important requirements for the realization of such a machine.

The foremost challenges for 15 T Nb₃Sn magnets include considerably larger coil volume, higher Lorentz forces and larger stored energy than in present accelerator magnets. The coil width, necessary to achieve the 15 T field level, requires 4-layer coil design [4]. The stronger forces produce higher stresses in the coil and in the mechanical structure and, thus, measures of stress control may be needed to keep stress and strain at an acceptable level for brittle Nb₃Sn conductor. The large stored energy also leads to complications in the magnet quench protection.

Fermilab has started the development of a 15 T Nb₃Sn dipole demonstrator for a 100 TeV scale HC based on the optimized "cos-theta" coil design [4], [5]. The experience gained at Fermilab during the Nb₃Sn accelerator magnet R&D for a Very Large Hadron Collider (VLHC) and the LHC upgrades [6], [7]

will be applied to all stages of the magnet design and fabrication. The main objectives of this magnet are demonstration of the 15 T field level in an aperture suitable for a future HC and study of the magnet quench performance and margins, quench protection and field quality. This paper describes the design concept and parameters of the 15 T Nb₃Sn dipole demonstrator developed at Fermilab. Magnetic and structural analyses as well as cable development and test results are also reported and discussed.

II. MAGNET DESIGN AND PARAMETERS

Five 4-layer graded coil cross-sections with 60-mm aperture were designed using ROXIE code [8] based on two cables with 15 mm width and thicknesses as listed in Table I [4]. The cables use 1.0 mm and 0.7 mm Nb₃Sn strands with a nominal critical current density J_c of 1500 A/mm² at 15 T and 4.2 K, and a nominal Cu/SC ratio of 1.13. Similar Nb₃Sn cables had already been developed at Fermilab and used in earlier dipole models [9], [10].

TABLE I
DIMENSIONS OF REACTED BARE CABLES.

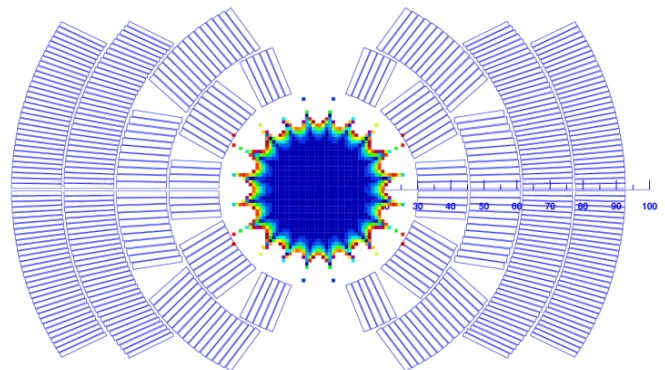| Parameter	Units	Cable 1	Cable 2
Number of strands		28	40
Mid-thickness	mm	1.870	1.319
Width	mm	15.10	15.10
Keystone angle	degree	0.805	0.805

Fig. 1. Coil cross-section with field quality diagram in the coil aperture. The dark colored zone represents a field uniformity better than 2×10⁻⁴.

Based on the design studies described in [4], a 4-layer 60-

mm aperture graded coil with optimized number of turns was selected for the 15 T dipole demonstrator. The selected coil cross-section is shown in Fig. 1. The two innermost layers have five blocks separated by 3 wedges. The two outermost layers do not use wedges. The large field harmonics generated by the two outermost layers were compensated by optimizing the number of turns and the wedge size and position in the two innermost layers. The resulting good field quality area in the aperture is shown in Fig. 1 by the dark colored zone.

The mechanical structure of the 15 T dipole demonstrator has been significantly reworked with respect to the original one described in [5] to address the large stress and deformation values revealed by ANSYS analysis. The new cold-mass structure of the 15 T dipole demonstrator is shown in Fig. 2.

The 4-layer coil assembly is surrounded by a 2 mm stainless steel spacer and supported by a vertically split iron yoke locked by aluminum clamps. The yoke is surrounded by a 12 mm thick stainless steel skin. The I-shaped clamps interleave with the iron yoke laminations in the top and bottom sectors of the iron yoke, thus reducing the iron filling factor in these areas to ~50%.

The axial Lorentz forces on the coil ends are intercepted by two thick end plates connected by eight stainless steel tie rods running through the dedicated holes in the iron yoke. This new support structure is different from the original concept based on stainless steel C-clamps and a thick skin [5]. It provides better stress management, as explained in the following section.

The magnet cold-mass is ~1 m long. The maximum cold mass transverse size is ~610 mm, which is limited by the inner diameter of the Fermilab test cryostat. Quench protection heaters composed of stainless steel strips are placed between the 2nd and 3rd coil layers and on the coil outer layer.
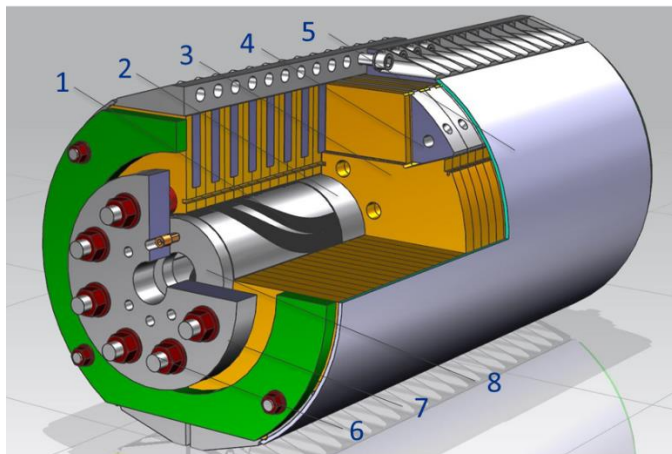

Fig. 2. Cold mass design of the 15 T dipole demonstrator: 1 – 4-layer Nb_3Sn coil; 2 – coil-yoke stainless steel spacer; 3 – iron yoke laminations; 4 – aluminum I-clamp; 5 – stainless steel bolted skin; 6 – axial tie rod; 7 – stainless steel end plate with instrumented bullets; 8 – pusher ring.

The calculated 2D design parameters of the 15 T dipole demonstrator are summarized in Table II. The field distribution diagrams in the coil and iron yoke are shown in Fig. 3. An iron filling factor of 50% in the area of the I-clamps was considered in the calculations. The maximum design bore field at 4.2 K is

15.6 T. Reducing the coil temperature to 1.9 K allows increasing the maximum bore field by ~10% with respect to the values shown in Table II.

TABLE II
MAGNET DESIGN PARAMETERS AT 4.2 K.

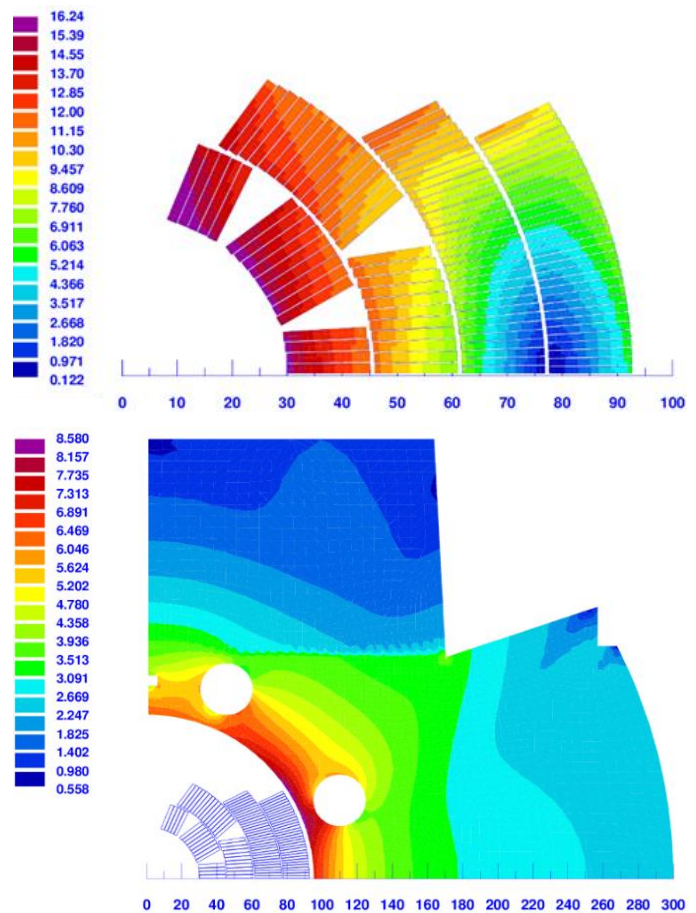| Parameter	Unit	Value
Bore field at short sample limit	T	15.61
Peak field at short sample limit	T	16.25
Current at short sample limit, I_c	kA	11.34
Inductance at I_c	mH/m	25.61
Stored energy at I_c	MJ/m	1.65
Horizontal Lorentz force per quadrant at I_c	MN/m	7.36
Vertical Lorentz force per quadrant at I_c	MN/m	-4.50

Fig. 3. 2D field distribution in the coil (top) and the iron yoke (bottom).

The geometrical harmonics in the magnet straight section at the reference radius of 17 mm are summarized in Table III.

TABLE III
NORMAL RELATIVE HARMONICS (10^{-4} OF THE DIPOLE COMPONENT)

Harmonic	Value
b_3	0.0018
b_5	0.0154
b_7	0.0523
b_9	0.0612

The calculated effects of superconductor magnetization and iron saturation on the "normal" relative sextupole field component b_3 as a function of dipole field in the magnet bore are shown in Fig. 4. The superconductor magnetization was calculated for a Nb₃Sn sub-element diameter of 52 µm in the two innermost layers (1 mm RRP-150/169 strand) and 41 µm in the two outermost layers (0.7 mm RRP-108/127 strand). The iron saturation effect was calculated for an iron having M_s of 2.14 T.
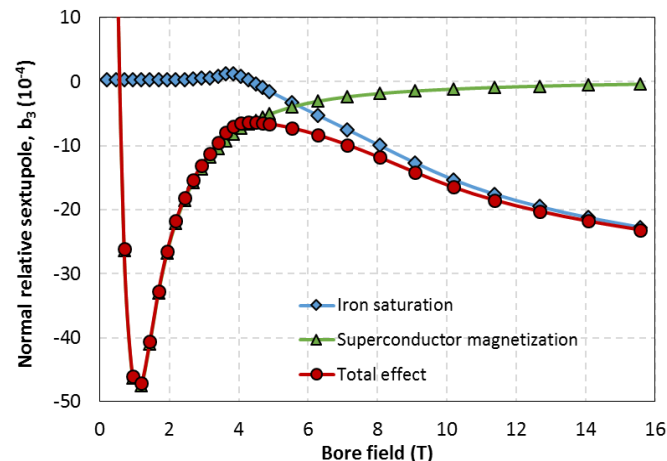

Fig. 4. Effects of superconductor magnetization and iron saturation on the normal relative sextupole b_3 during current ramp-up in the second excitation cycle.

Due to large coil volume, high J_c and large Nb₃Sn sub-element size the superconductor magnetization effect in the normal sextupole component b_3 in the 15 T demonstrator is large. The absolute peak value of b_3 reaches ~48 units at a bore field of ~1 T. It is a factor of two larger than in the 2-layer 11 T dipole where it attains ~20 units [11], and an order of magnitude larger than in the NbTi LHC main dipoles. Since the iron yoke is close to the coil in the 15 T dipole demonstrator, the iron saturation effect is also large. The variation of the normal sextupole b_3 due to the iron saturation in the 15 T dipole demonstrator is more than 20 units.

No special field quality correction is envisioned for the first 15 T dipole demonstrator since it will be used to measure the unaltered, weakly-coupled coil magnetization and iron saturation effects, and to benchmark the computation codes. For future models, a persistent current corrector, similar to that developed for previous magnets [12], will be considered in conjunction with optimizing holes in the iron yoke – the techniques also previously used at Fermilab [13] to further suppress both non-linear effects.

The 3D magnetic analysis was performed using the OPERA 3D code. Fig. 5 shows the complete 4-layer coil and the coil end design. The length of both ends of the two outermost layers was minimized in order to increase the length of the magnet straight section. Small end spacers were used in these layers to split the large blocks and reduce the accumulated turn inclination. For mechanical reasons the iron yoke is extended over the coil ends. In that case, the peak field point limiting the magnet performance is in the coil ends. To reduce the field enhancement in the coil ends with respect to the magnet straight

section, the pole blocks of the two innermost layers were shifted towards the magnet center.
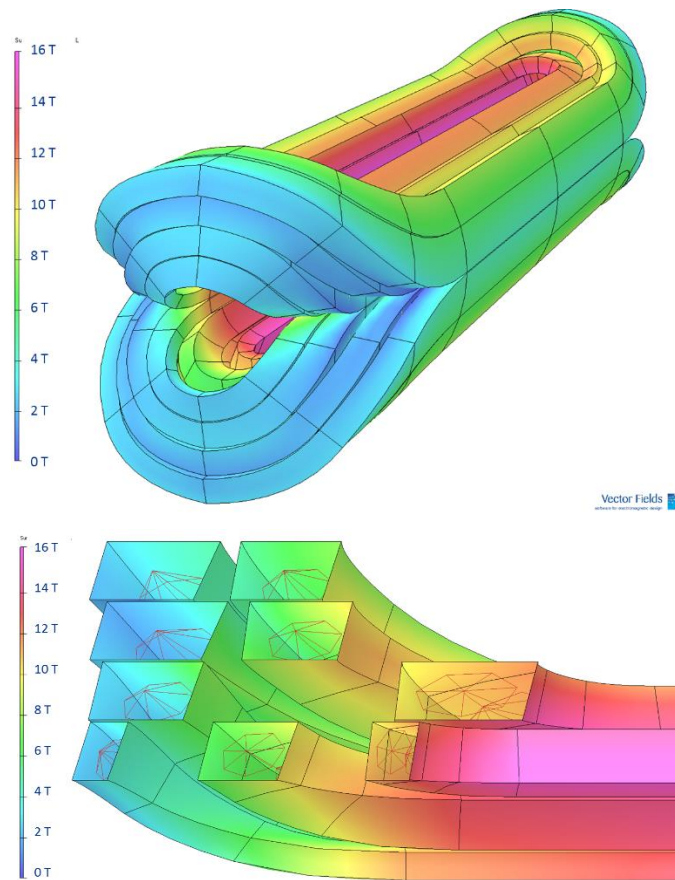

Fig. 5. Complete coil (top) and the coil end cross-section (bottom) with the magnetic flux distribution at the magnet short sample limit.

A cylindrical cut-out was also introduced in the ends of the iron yoke, as shown in Fig. 6, to reduce the peak field in the coil ends. There is a 2% field enhancement in the coil ends without the cutout. Removing ~45 mm of the iron yoke material around the coil ends helps to reduce the peak field in the end to the same level as in the magnet central cross-section.
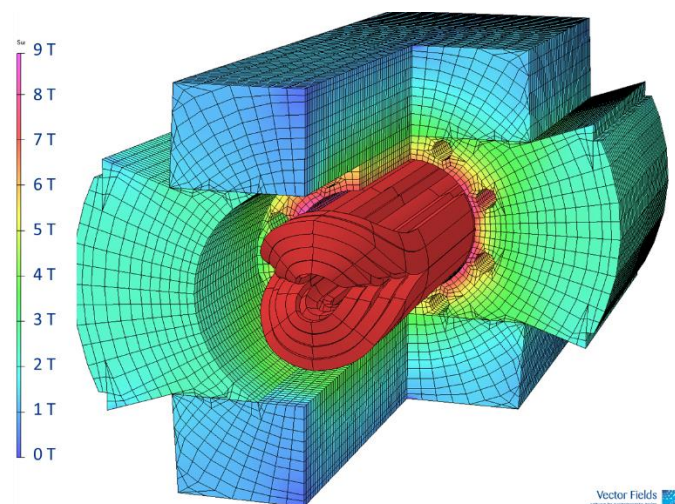

Fig. 6. 3D model with flux density in the iron yoke at the short sample limit.

The coil cross-sections, optimized with ROXIE, were input into the BEND program [14] where the three-dimensional end geometry of each group was optimized by minimizing the strain energy in the cables with respect to "bend in the hard direction", providing also the information on turn twist and radius of curvature. Slight shifting and manual adjustments of the BEND parameters were done to produce a cable geometry that does not require bottom-supporting parts. The output files from BEND were then directly imported into a CAD package. The completed CAD geometry can then be imported into other programs for magnetic field and coupled mechanical and thermal FEA.

Fig. 7 shows the end geometry (top) and corresponding end parts (bottom) for both lead and return ends of the innermost coil layer. Fig. 8 shows the two outermost layers of the coil. The 2-layer inner coil uses Ti-alloy poles, bronze wedges and end spacers, and stainless steel saddles. All parts of the 2-layer outer coil are made of stainless steel.
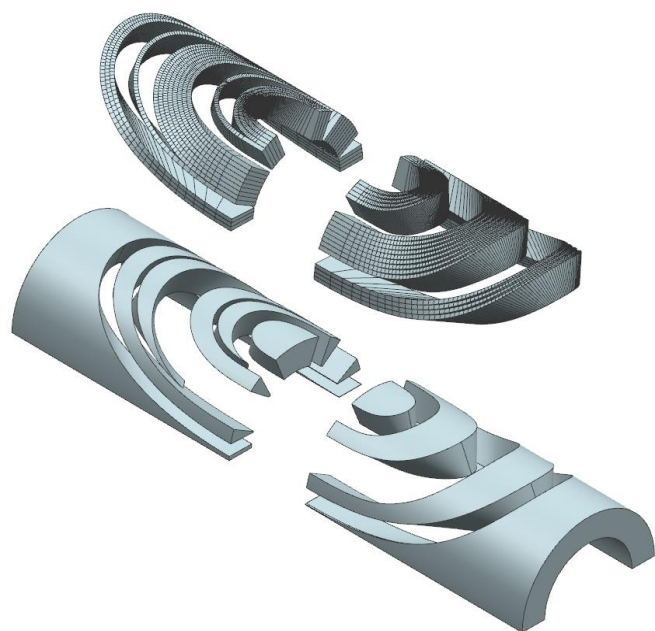
Fig. 7. The end geometry of the innermost coil layer (top) and corresponding end parts (bottom). The left and right sides of the Figure correspond to the lead ends and return ends respectively.
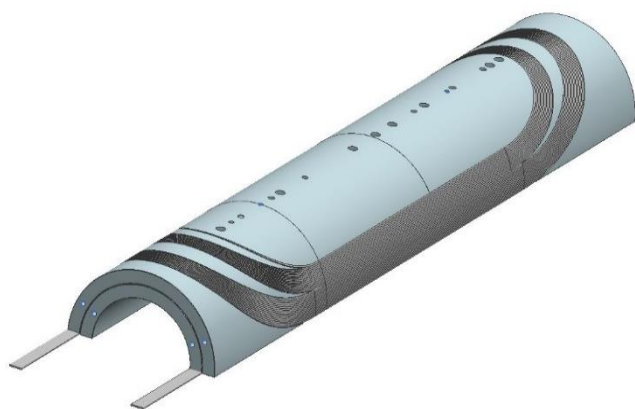
Fig. 8. The two outermost layers of the coil.

III. STRUCTURAL ANALYSIS

Finite element analysis using a parametric 2D ANSYS model was performed to optimize the stress in the coil and the main elements of the magnet support structure, and to minimize the conductor motion and magnet cross-section deformation at room and operation temperatures up to the design field of 15 T.

The ANSYS model of the 15 T dipole demonstrator in two cross-sections is shown in Fig. 9. The baseline materials used in the magnet and their properties are listed in Table IV. The data for the Nb_3Sn coil are based on measurements reported in [15]. The key criteria of the mechanical optimization were a) maintaining the coils under compression up to the design field of 15 T, and b) keeping the maximum coil stress below ~180 MPa during magnet assembly and operation.
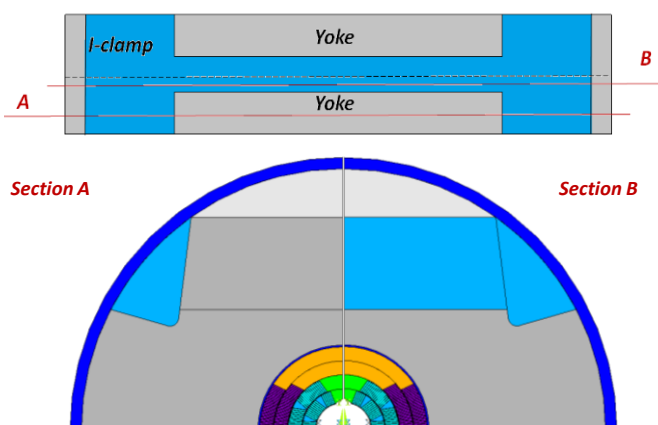
Fig. 9. ANSYS model of 15 T dipole (bottom) for section A (left) and section B (right) shown on the top sketch.

TABLE IV
MATERIAL PROPERTIES.

Structural element	Material	Thermal contract. (300-2 K), mm/m	Elasticity modulus, GPa		Yield stress, MPa	
			warm	cold	warm	cold
Coil (rad/azim)	Nb_3Sn composite	2.9/3.3	35/20	40/40	n/a	n/a
Inn.coil pole blocks	Ti-6Al-4V	1.7	115	125	650	>900
Out.coil pole blocks	St Steel	2.9	195	215	230	500
Wedges	Bronze	3.2	110	120	280	350
Coil-yoke spacer	St Steel	2.9	190	210	230	500
Clamp	Aluminum	4.1	70	81	500	600
Yoke	Iron	2.0	210	225	350	>400
Skin	St Steel	2.9	190	210	230	500

Distributions of the equivalent stress in the coil after assembly, after cooling down and at 15 T bore field are shown in Fig. 10. The average transverse (azimuthal) stress in the pole and mid-plane turns of the coil layers at the above stages is summarized in Table V. The maximum equivalent coil stress at room temperature and after cooling down is ~110 MPa and ~150 MPa respectively in the innermost-layer pole turn. The prestress increase in the pole-turns is achieved by providing the proper gap between the two halves of the iron yoke during assembly. The gap is closed after cooling down and stays closed up to 15 T. At the bore field of 15 T, the maximum equivalent coil stress is in the innermost layer mid-plane turns and is close to 178 MPa.
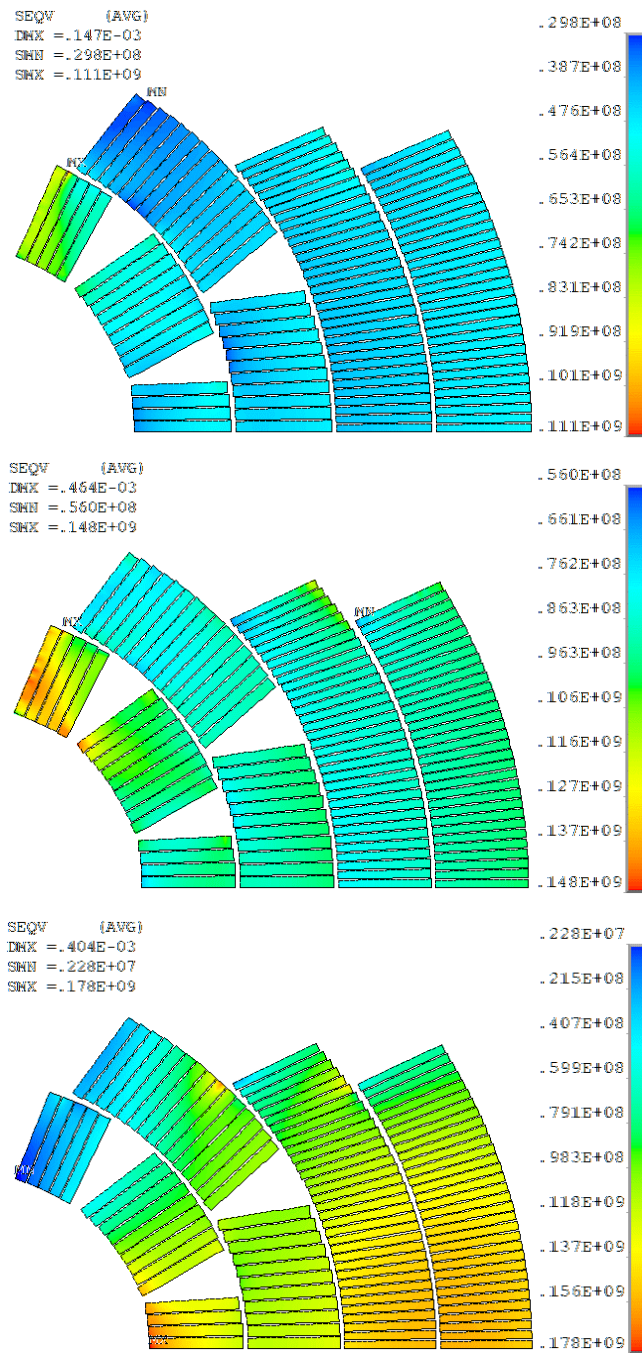
Fig. 10. Equivalent stress distribution in the coil at room temperature after assembly (top), after cooling down (middle) and at the 15 T bore field (bottom).

TABLE V
AVERAGE AZIMUTHAL STRESS IN SELECTED TURNS.

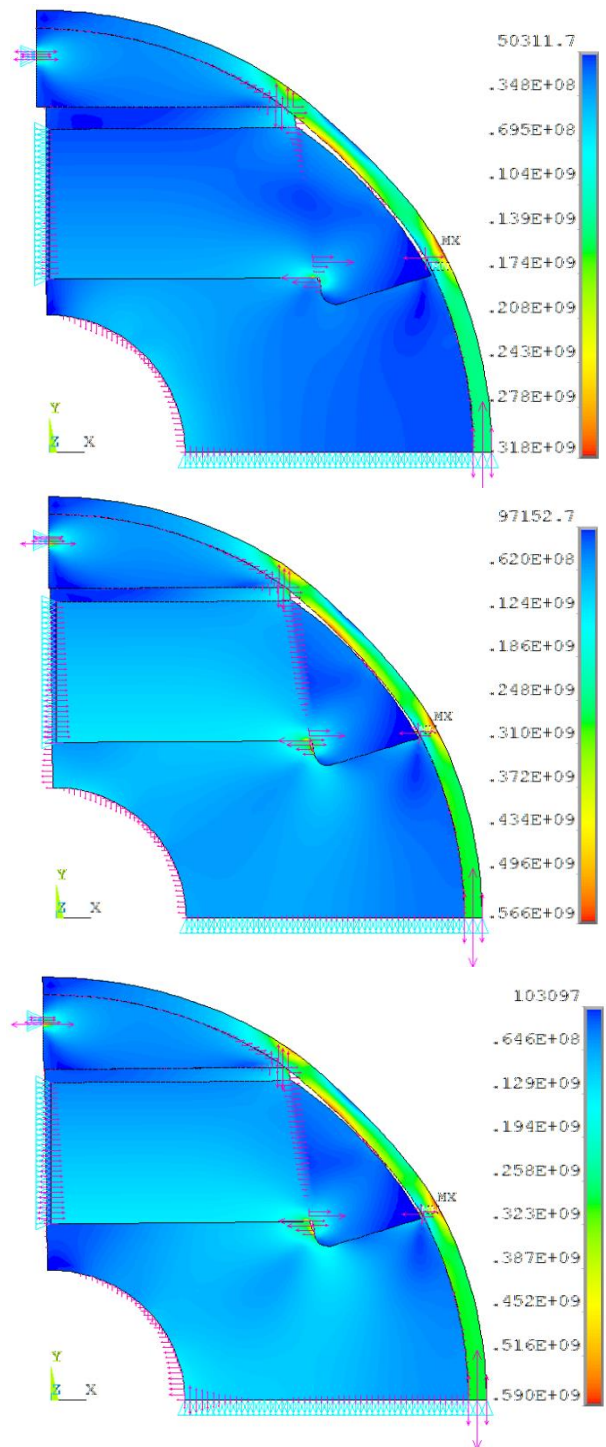| Position in coil	Azimuthal coil stress, MPa		
	Assembly	Cool down	B=15 T
Pole 1	73	131	3
Pole 2	36	82	24
Pole 3	53	99	36
Pole 4	51	100	66
Mid-plane 1	50	97	155
Mid-plane 2	53	107	124
Mid-plane 3	51	95	155
Mid-plane 4	55	106	156

Fig. 11. Equivalent stress distribution in the support structure at room temperature after assembly (top), after cooling down (middle) and at 15 T bore field (bottom).

TABLE VI
MAXIMUM EQUIVALENT STRESS IN KEY STRUCTURAL ELEMENTS (MPA).

Structural element	Maximum stress, MPa		
	Assembly	Cool down	B=15 T
Yoke	210	360	490
Clamp	205	430	450
Skin	318	566	590

Distributions of the equivalent stress in the dipole mechanical structure are shown in Fig. 11. The maximum values of the equivalent stress in the major elements of the magnet support structure, which were calculated at different assembly and operation stages, are presented in Table VI. All the results were obtained using a conservative model with elastic material properties. The stress level in clamps, iron laminations and skin during magnet assembly and operation are at an acceptable level for the materials used.

IV. CABLE OPTIMIZATION

The 40-strand Rutherford cable used in the two outermost coil layers was developed and optimized for the 11 T LHC dipole [9]. No additional optimization was needed for this cable. Three unit lengths of this cable with 0.7 mm diameter RRP-108/127 strands are presently available for the outer coils of the 15 T demonstrator dipole. A cross-section of the 40-strand Rutherford cable is shown in Fig. 12 (top).
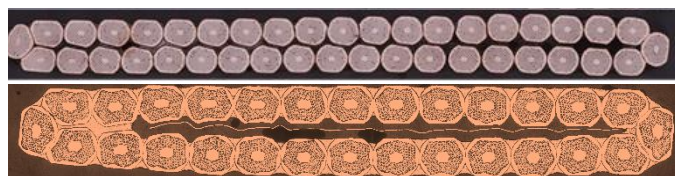

Fig. 12. Cross-sections of the 40-strand (top) and 28-strand (bottom) Rutherford cables.

The Rutherford cable with 28 strands of 1 mm diameter and 14.7 mm nominal width before reaction was optimized for the 15 T dipole demonstrator using state-of-the-art RRP® wires. A cross-section of the optimized 28-strand Rutherford cable is shown in Fig. 12 (bottom).

The cable samples were fabricated in one pass. They all included an 11 mm wide 0.025 mm thick stainless steel core to suppress eddy currents and obtain better field quality and ramp rate dependence in magnets. The first series of cable samples made of RRP-108/127 strands demonstrated critical current degradation smaller than 4% over the whole range of packing factors up to 92% encompassed by the cables [16]. Then cable degradation studies were continued with a RRP-150/169 wire most recently procured for the 15 T dipole demonstrator.

The critical current I_c at 4.2 K normalized to the average I_c of the virgin wires (PF=78.5%) is plotted in Fig. 13 as a function of cable packing factor for two different external field values. The I_c degradation was less than 3% for cables up to ~90% cable compaction.

The Residual Resistivity Ratio (RRR) was measured as the ratio of the wire resistivity at room temperature over its residual resistivity at 19.5 K. Fig. 14 shows the RRR as a function of PF for the RRP-150/169 extracted strands. The overall RRR of the wires decreased more or less linearly with compaction and was more than 250 up to ~90% cable compaction.

Based on these results, the nominal mid-thickness of the inner-coil unreacted cable that was chosen for the 15 T dipole is 1.80 mm.

The $I_c(B)$ dependences, measured using extracted strands at 4.2 K, and calculated for 4.5 and 1.9 K using parameterization [17] for the 28-strand cable, as well as the 15 T dipole

demonstrator load lines (LL) are shown in Fig. 15. The magnet short sample limits estimated based on these data are 11.05 kA (B_0=15.25 T) at 4.5 K and 12.2 kA (B_0=16.65 T) at 1.9 K, which is consistent with the design parameters shown in Table II.
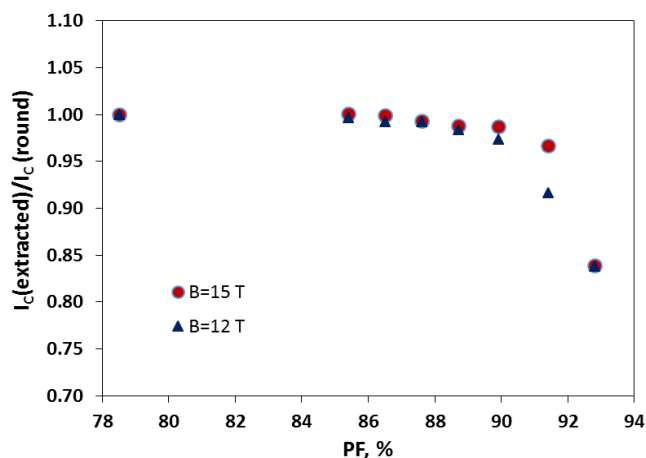

Fig. 13. Extracted strand I_c at 4.2 K normalized to I_c of virgin wire vs. cable packing factor for cables made with RRP-150/169 Nb_3Sn strands.
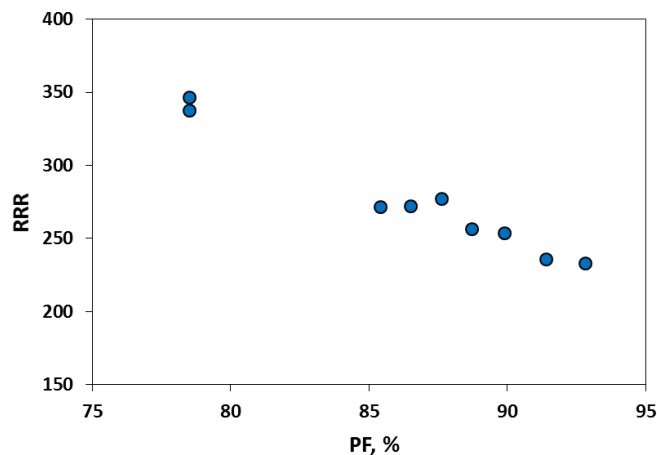

Fig. 14. RRR as a function of cable packing factor for RRP-150/169 strands.
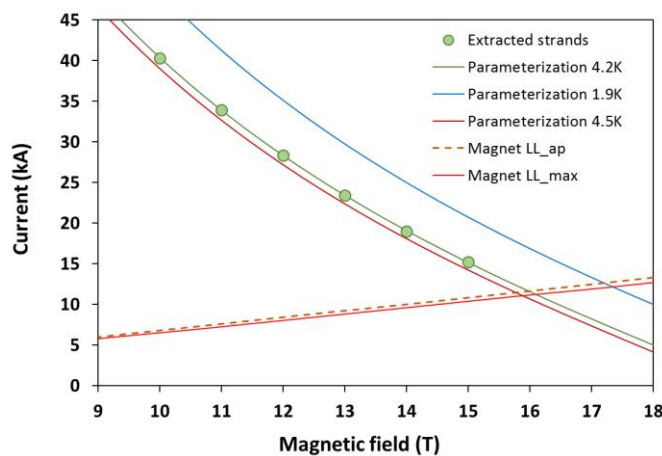

Fig. 15. Measured and parameterized $I_c(B)$ dependences for the 28-strand cable and 15 T dipole demonstrator load lines (LL). The LL_ap and LL_max represent the magnetic field in the magnet aperture and the maximum field in the coil respectively as function of magnet current.

V. Conclusions

A 15 T Nb$_3$Sn dipole demonstrator for a future HC is being developed at Fermilab. Magnet design is based on a 4-layer graded block cos-theta coil with 60 mm aperture and cold iron yoke. The magnet maximum field estimated based on the cable data is 15.25 T at 4.5 K and 16.65 T at 1.9 K.

There are large non-linear superconductor magnetization and iron saturation effects in the sextupole field component. No special field quality correction is envisioned for the first 15 T dipole demonstrator. Tuning of the field quality using various techniques will be explored in future models.

The magnet support structure has been optimized to manage the large level of Lorentz forces. The concept has been radically changed from the previous iteration, which revealed excessively high stresses in the magnet structure and a possible separation of the pole turns at the maximum field. It was shown that the new structure allows keeping the stresses in the coil and support structure within acceptable limits during magnet assembly and operation.

Cable samples for both inner and outer coils were fabricated and tested. The cable packing factor was optimized to achieve a low degradation of cable critical current and copper matrix conductivity. The design of a 4-layer coil, including coil ends, mechanical structure and tooling is complete and being procured. Magnet fabrication and first test are planned for 2016.

Acknowledgement

References

[1] "Building for Discovery: Strategic Plan for U.S. Particle Physics in the Global Context," P5 Report, http://science.energy.gov/~/media/hep/hepap/pdf/May%202014/FINAL _P5_Report_053014.pdf

[2] Future Circular Collider Study Kickoff Meeting, Geneva, Switzerland, February 12-14, 2014, http://indico.cern.ch/event/282344/timetable/#20140212

[3] CEPC/SppC study in China, http://indico.cern.ch/event/282344/session/1/contribution/65/material/sli des/1.pdf

[4] A.V. Zlobin et al., "Design concept and parameters of a 15 T Nb$_3$Sn dipole demonstrator for a 100 TeV hadron collider," Proc. of IPAC2015, Richmond (VA), May 2015.

[5] V.V. Kashikhin et at., "Magnetic and structural design of a 15 T Nb$_3$Sn accelerator dipole model," Proc. of CEC/ICMC2015, Tucson (AZ), 2015. *IOP Conf. Ser.: Materials Science and Engineering (MSE), submitted for publication.*

[6] A.V. Zlobin, "Status of Nb$_3$Sn Accelerator Magnet R&D at Fermilab", EuCARD - HE-LHC'10 AccNet mini-workshop on a "High-Energy LHC", 14-16 October 2010, FERMILAB-PUB-11-001-TD, CERN Yellow Report CERN-2011-003, p. 50 [arXiv:1108.1869].

[7] A.V. Zlobin et al., "11 T Twin-Aperture Nb$_3$Sn Dipole Development for LHC Upgrades," *IEEE Trans. Appl. Supercond.*, v. 25, Issue 3, June 2015, 4002209.

[8] ROXIE Code for an Electromagnetic Simulation and Optimization of Accelerator Magnets, http://cern.ch/roxie.

[9] N. Andreev et al., "Development of Rutherford-type Cables for High Field Accelerator Magnets at Fermilab," *IEEE Trans. Appl. Supercond.*, v. 17, Issue 2, June 2007, p. 1027.

[10] E. Barzi et al., "Development and Fabrication of Nb$_3$Sn Rutherford Cable for the 11 T DS Dipole Demonstration Model," *IEEE Trans. Appl. Supercond.*, v. 22, Issue 3, June 2012, 6000805.

[11] B. Auchmann et al., "Magnetic Analysis of a Single-Aperture 11T Nb$_3$Sn Demonstrator Dipole for LHC Upgrades", Proceedings of IPAC2012, New Orleans, Louisiana, USA, p. 3596.

[12] V.V. Kashikhin et al., "Passive Correction of the Persistent Current Effect in Nb$_3$Sn Accelerator Magnets," *IEEE Trans. Appl. Supercond.* vol. 13, no. 2, June 2003, p. 1270.

[13] G. Ambrosio et al., "Magnetic Design of the Fermilab 11 T Nb$_3$Sn Short Dipole Model," *IEEE Trans. Appl. Supercond.* vol. 10, no. 1, March 2000, p. 322.

[14] J. M. Cook, "Strain Energy Minimization in SSC Magnet Winding," *IEEE Trans. on Magnetics*, vol. 27, March 1991, p.1976.

[15] D. R. Chichili et al., "Investigation of Cable Insulation and Thermo-Mechanical Properties of Epoxy Impregnated Nb$_3$Sn Composite," *IEEE Trans. on Applied Supercond.*, vol. 10, no. 1, 2000, p. 1317.

[16] E. Barzi et al., "Nb$_3$Sn RRP® Strand and Rutherford Cable development for 15 T Accelerator Magnets," *this conference.*

[17] L.T. Summers et al., "A model for the prediction of Nb$_3$Sn critical current as a function of field, temperature, strain and radiation damage", *IEEE Trans. on Magnetics*, 27 (2): 2041-2044 (1991).